[Research Paper] 대한금속 · 재료학회지 (*Korean J. Met. Mater.*), Vol. 59, No. 8 (2021) pp.524-532
DOI: 10.3365/KJMM.2021.59.8.524

Effect of Low Transformation Temperature Welding Consumable on Microstructure, Mechanical Properties and Residual Stress in Welded Joint of A516 Carbon Steel

Sungki Choi[1,†], Junsang Lee[1,†], Jae-Yik Lee[2], Seung-Kyun Kang[1], Young-Cheon Kim[3,*], Seung-Joon Lee[4,], and Dongil Kwon[1]**

[1]*Department of Materials Science and Engineering, Seoul National University, Seoul 08826, Republic of Korea*
[2]*Welding & Joining Research Group, Steel Solution Research Lab, Technical Research Lab., POSCO, Pohang 37859, Republic of Korea*
[3]*Research Center for Energy and Clean Technology, School of Materials Science and Engineering, Andong National University, Andong 36729, Republic of Korea*
[4]*Department of Advanced Materials Engineering, Korea Polytechnic University, Siheung 15073, Republic of Korea*

Abstract: The microstructure, mechanical properties and residual stress of flux-cored arc welded ASTM A516-70N carbon steel using a Mn-based low-temperature transformation (LTT) welding consumable were investigated. Microstructural analysis with X-ray diffraction, an electron backscattered diffractometer and a field-emission scanning electron microscope showed that the LTT weld metal was made up of ferrite, austenite, martensite, and bainite with phase fractions 50.5%, 0.2%, 40.2% and 9.1%, respectively. The increase in hardness and the decrease in absorbed impact energy of the LTT weld metal compared with conventional consumable welds were confirmed to be due to the relatively high fraction of martensite phase in the weld metal. The welding residual stress distributions in three coupons (LTT, conventional and post-weld heat-treated conventional weld) were compared by the results using instrumented indentation testing. The LTT weld coupon showed compressive residual stress distributed in the weld metal and heat-affected zone (HAZ), confirming previous studies in which this residual stress was attributed to a martensitic phase transformation at relatively low temperature. PWHT in the conventionally welded coupon considerably reduced the tensile residual stress distributed in the weld metal and HAZ. The LTT consumable, however, showed a significant advantage in welding residual stress, even compared with the heat-treated conventional consumable.

(Received April 6, 2021; Accepted April 29, 2021)

Keywords: low transformation temperature, LTT consumable, flux-cored arc welding, mechanical properties, residual stress, indentation

1. Introduction

The integrity of welds in various industrial processes such as building construction, ships, automobiles, mining is crucial to the overall safety of the structure. In particular, tensile residual stresses introduced by the welding process can affect in the entire stress state of the weld. Welding residual stress, which is inevitable during cooling after welding, can lead to stress-corrosion cracking, distortion, and reduction in the fatigue strength of the weldment [1-5]. Several thermal and mechanical techniques can reduce the tensile residual stresses in the joint via introducing compressive residual stresses. These include post-weld heat treatment (PWHT), shot peening and thermal tensioning techniques [6-11]. However, these methods have limitations such as technical complexity, high cost and time-consuming process.

Many studies have been carried out on ways to reduce residual stresses and improve the mechanical properties of weldments using novel welding consumables that can control

-
**Corresponding Author:* Young-Cheon Kim
[Tel: +82-54-820-6810, E-mail: kimyc@anu.ac.kr]
***Corresponding Author:* Seung-Joon Lee
[Tel: +82-31-8041-0585, E-mail: leesj@kpu.ac.kr]
+These authors contributed equally to this work

the processing temperature, preventing the phase transformation. Alberry and Jones reported that a reduction in processing temperature can drive the suppression of residual stresses [12]. Low-transformation-temperature (hereinafter LTT) welding consumables that exploit this phenomenon have been developed in recent years [13-17]. Conventional consumables have a transformation temperature of about 500 ºC, but in an LTT welding material with Fe-10Ni-10Cr (wt.%) developed by Ohta *et al*., phase transformation occurred at 180 ºC [14]. This welding consumable could reduce tensile residual stresses or generate compressive residual stresses. Kromm and Kannengiesser reported that the martensite start temperature (Ms) decreased with increasing Ni content due to the higher austenite (γ) stability [18]. Murakawa *et al*. reported that compressive residual stress increased as Ms decreases up to approximately 200 ºC [6]. Many researchers have found not only a reduction in residual stress but also an improvement in fatigue strength [17,19-22] and the suppression of distortions [23-26] in weldments when using LTT welding materials. By tuning the temperature so that the transformation from γ to α'-martensite occurs at a lower temperature, the volume expansion accompanied by strain can compensate thermal shrinkage that occurs with cooling after welding [14,27,28].

Figure 1(a) and (b) show the variation in strain and stress in a conventional consumable and a LTT consumable during cooling, respectively. The two welding materials differ in the conventional consumable, and shrinkage is a dominant factor after the expansion due to phase transformation from γ to α' phase at 500 ºC (Figure 1(a)). This results in a tensile residual stress at room temperature (Figure 1(b)). On the other hand, the expansion from 200 ºC to room temperature is dominant in the weld using the LTT consumable, because the phase transformation occurs at a relatively low temperature of 200 ºC (Figure 1(a)), leading to compressive residual stress (Figure 1(b)).

Automating the welding process is essential for efficiency in an industry that requires in-field and large-scale applicability. Flux-cored arc welding (FCAW) is preferred, to ensure weld quality and to reduce labor costs. This automatic or semi-automatic technique is widely used in shipbuilding, manufacturing and repair welding, because it provides high productivity and industrial applicability compared to other methods such as shield metal arc welding (SMAW) and friction stir welding. As noted above, using LTT consumables can induce compressive residual stress, so the PWHT process for relieving residual stresses can be eliminated and productivity can be increased by utilizing LTT with FCAW.

In this study, the effect of a low-temperature-transformation (LTT) consumable using FCAW on ASTM A516-70N carbon steel was analyzed quantitatively with respect to microstructure, mechanical properties and residual stress. Electron backscattered diffractometer and field-emission scanning electron microscope were used to characterize the microstructure of the LTT weld metal compared to a conventional weld metal. Micro Vickers hardness and impact toughness tests evaluated the effect of changes in microstructure on mechanical properties. The LTT consumable showed a strong advantage in welding residual stress over conventional weld coupons. The effect of the welding consumable was confirmed to be superior to the residual stress relaxation effect of PWHT.

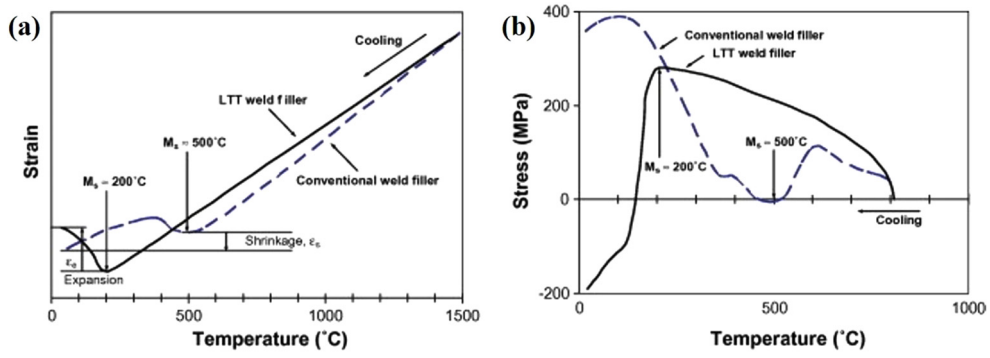

Fig. 1. Variation of strain and stress during cooling process: (a) strain and (b) stress [27].

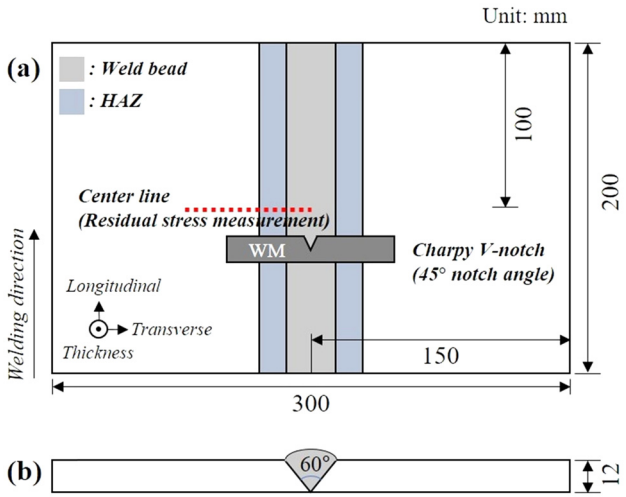

Fig. 2. Schematic layout of welding coupons from (a) top view, (b) side view and Charpy impact test specimen.

2. Experimental Procedure

2.1 Materials and weld fabrication

A schematic layout of the welded coupons is shown in Fig. 2. The chemical composition carbon equivalent (C_{eq}) of welding consumables and base metal is listed in Table 1, and their mechanical properties are presented in Table 2. The carbon equivalent of the welding materials can be calculated with Eq. (1) [29].

$$C_{eq} = C + \frac{Mn}{6} + \frac{(Cr+Mo+V)}{5} + \frac{(Ni+Cu)}{15} \quad (1)$$

Welding plates of ASTM A516-70N carbon steel were prepared for a butt weld size of 300 mm^w × 200 mm^l × 12 mm^t (two plates 150 mm wide were joined), which had a 60 º V-groove geometry. Welding consumables with 1.2 mm diameter, AWS E71T-1C [30] were used for the conventional welding coupon and Mn-based LTT material for the LTT welding coupon, were welded in four passes. Flux-cord arc welding (FCAW) was performed with different welding conditions and two welding consumables, as shown in Table 3. Three FCAW coupons were fabricated, two with conventional consumables and one with a Mn-based LTT consumable. One of the conventional welding coupons was post-weld heat-treated as specified in ASME section III NX-4622 [31]. PWHT was performed at 635±15 ºC for 12 hours after welding, according to ASME section III NX-4622 [31], for an additional conventional welding coupon.

Table 2. Tensile properties of welding consumables and base material

Materials	Yield strength (MPa)	Tensile strength (MPa)	Elongation (%)
Conventional consumable	520	580	23
Mn- LTT consumable	727	820	23
Base metal (A516-70N)	404	575	21

Table 3. Welding conditions for welding consumables

	Welding current (A)	Arc voltage (V)	Welding speed (cm/min)	Heat input (kJ/cm)
Conventional consumable	240	30	22	20
Mn- LTT consumable	260	32	48	10

2.2 Microstructure characterization and mechanical properties

Cross-sectional samples of 10 mm^w × 10 mm^l × 10 mm^t containing the fusion line were machined at the center of the welding coupons from the LTT weld and the conventional weld without PWHT. The samples were mechanically polished with 400-2400 grit paper and then a suspension with 1-μm-diamond particles and 0.25-μm-colloidal silica. X-ray diffractometer (D8-Advance, Bruker, Karlsruhe, Germany) was used to detect the phases of the weld metal with the two welding consumables using a Cu-Kα target, and a scanning range and speed of 20 º to 100 º and 3 º/min, respectively.

The sample used for X-ray diffraction measurement was chemically etched with 5% nital for microstructural observation. A field-emission scanning electron microscope (FE-SEM, FEI Quanta 250 FEG, Hillsboro, OR, USA) was used to identify the microstructures in the weld metal. Additional

Table 1. Chemical compositions and carbon equivalent (C_{eq}) of welding consumables and base material (wt-%)

	C	Si	Mn	O	P	S	Fe	C_{eq}
Conventional consumable	0.04	0.55	1.25	-	0.02	0.01	Bal.	0.25
Mn- LTT consumable	0.03	0.38	4.30	0.07	-	-	Bal.	0.75
Base metal (A516-70N)	0.31	0.15-0.40	0.85-1.20	-	0.03	0.03	Bal.	0.45-0.51

surface preparation was made for electron backscattered diffractometer (EBSD; EDAX-Hikari) analysis by electropolishing in a mixed solution of 90% ethanol (C_2H_5OH) and 10% perchloric acid ($HClO_4$) at 31 V for 30 s. EBSD analysis was operated at an acceleration voltage of 15 kV and a working distance of 15 mm, and a step size of 2 μm. The phase fraction in the weld metal with the LTT consumable was analyzed quantitatively under this condition with a scan area of 200 μm × 200 μm and a step size of 0.5 μm.

Microhardness testing was performed by Micro-AIS (Frontics Inc., Seoul, Korea) with a Vickers indenter at fixed maximum load of 0.1 kgf. The hardness distribution over the cross-section was measured from the weld center toward the heat-affected zone (hereinafter HAZ). Two diagonal lengths of the indent were directly measured by optical microscope. Three sub-sized Charpy V-notch specimens (5 mm × 10 mm × 55 mm, 45 °) were extracted from the center of the weld line following ASME section II SA370 [32] in the direction transverse from the welding plates, as shown in Fig. 2. The tests were conducted at room temperature

2.3 Residual stress measurement

The residual stress of the LTT welding coupon was measured using X-ray diffraction prior to indentation testing to compare the results of the two tests. An Xstress3000 (X-ray Stress Analyzer) was used with Cr-Kα radiation (λ = 0.22911 nm), 2θ = 156.4 °, diffracting plane {211} from base metal and weld metal. From Bragg's Law, the sin2ψ method was used for measurements. To measure the changes in lattice spacing, the operating voltage was 30 kV and the current 6.7 mA. The measurements were carried out from the weld center through the red line (Fig. 2) perpendicular to the welding line at 2 mm intervals.

Instrumented indentation testing (IIT) was performed for residual stress measurement on the top surface of the three welding coupons, carefully polished up to 2000 grit sandpaper following ISO 14577-1 [33]. A commercial indentation system, AIS 3000 (Frontics Inc., Korea) with a load resolution of 0.05 N and depth resolution of 0.1 μm was used. A Vickers indenter with an apex angle of 136 ° [34] was used, and all the tests were controlled with a maximum load of 490 N (50 kgf) and an indentation loading rate of 0.3 mm/min. The measurements were performed at 4 mm intervals on the red line, as well where the X-ray diffraction was performed. The normality between the indenter and the specimen surface was carefully controlled not to exceed 1 degree.

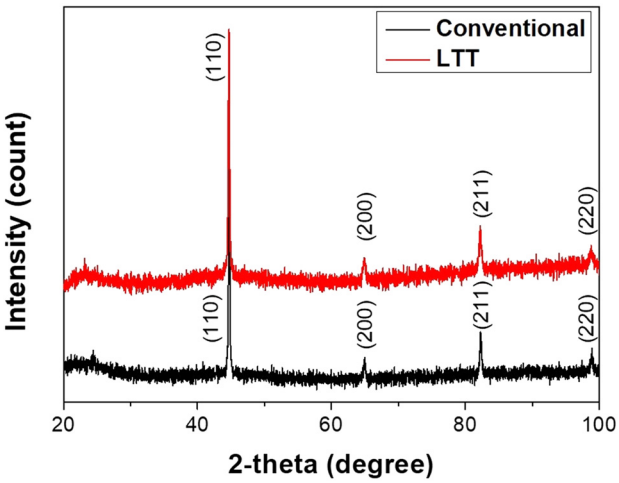

Fig. 3. Results of XRD in weld metal of conventional and LTT consumable.

The model developed by Lee and Kwon was used for residual stress evaluation [35]. The indentation load-depth curve is shifted depending on the sign and magnitude of the residual stress relative to the curve in the stress-free state. The relation between the force difference as a result of residual stress and the deviatoric stress of the indenting direction was formulated with the projected area as Eq. (2).

$$\sigma_{residual} = 3 \cdot \frac{(L_0 - L_s)}{A_s} \tag{2}$$

where L_0 and L_s are the loads in the stress-free and stressed state, respectively, and A_s means indentation contact area.

3. Results and Discussion

3.1 Microstructure characterization

The microstructure of the LTT weld metal was characterized by X-ray diffraction, FE-SEM and EBSD, and then compared to the conventional weld metal without PWHT. The X-ray diffraction peaks of the two weld metals (except the conventional weld metal with PWHT, since phase transformation does not generally occur with PWHT) are compared in Fig. 3. Both weldments had phases suspected to be ferrite or bainite/martensite showing a bcc structure in the

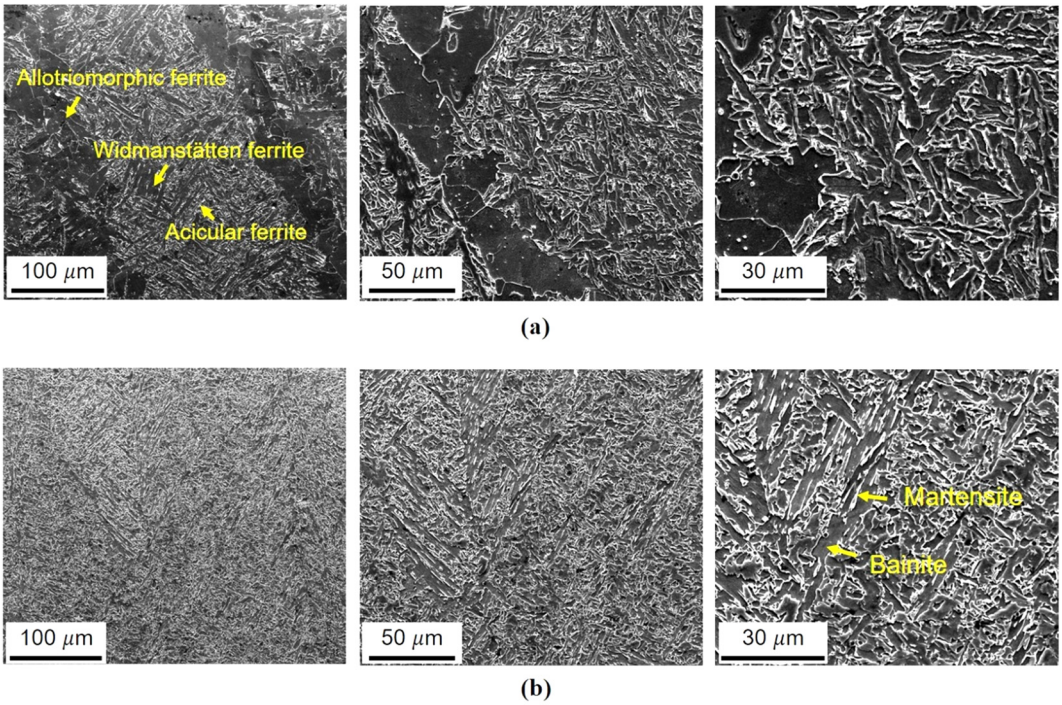

Fig. 4. FE-SEM Micrographs in weld metal of sample welded with (a) conventional and (b) LTT consumables.

weld metal. No retained austenite phase was detected by X-ray diffraction analysis; it rarely forms when the carbon content is less than 0.4 wt% [36], as was the cases in these two weldments.

Figure 4 shows the weld metal images obtained from FE-SEM at ×800, ×1500 and ×3000 magnitude. Ferrite phases (acicular, allotriomorphic, and Widmanstätten) were observed in the weld metal with the conventional consumable, as previously reported [37,38]. And, in case of the weldment with the LTT, mixed structures of ferrite, bainite, and martensite were detected. These results correspond to those of the X-ray diffraction peak analyses.

For more depth-in-analysis of phases in the conventional and LTT welding, the effective grain size and phase fraction of the weld metals was measured by EBSD analysis. Figure 5 shows the IQ map of the weld metals. The average effective grain size can be calculated by defining a misorientation angle larger than 15 ° [39,40]. The average effective grain sizes were 6.70 μm and 5.49 μm for the conventional and LTT consumable, respectively. It was estimated that the maximum temperature during welding of the conventional consumable was higher than the LTT consumable, and LTT's

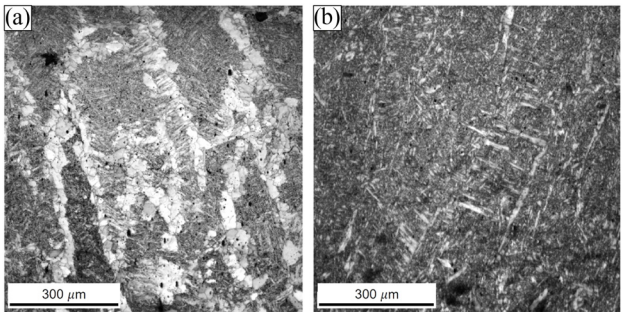

Fig. 5. IQ map of sample welded with (a) conventional and (b) LTT consumables in weld metal.

finer effective grain size affected the hardness and impact toughness.

GOS map and Gaussian fitting graph from IQ analysis using EBSD were performed for the LTT consumable, since the phases were difficult to distinguish accurately using only XRD and FE-SEM. The fraction of martensite phase in the weld metal of the Mn-based LTT consumable was distinguished by analyzing the grain orientation spread (GOS) map and IQ map from the EBSD results. Low-angle and high-angle boundaries were divided by ranges into $2° < \theta < 15°$ and $\theta > 15°$ [41] and are indicated in Fig. 6(a) as red and

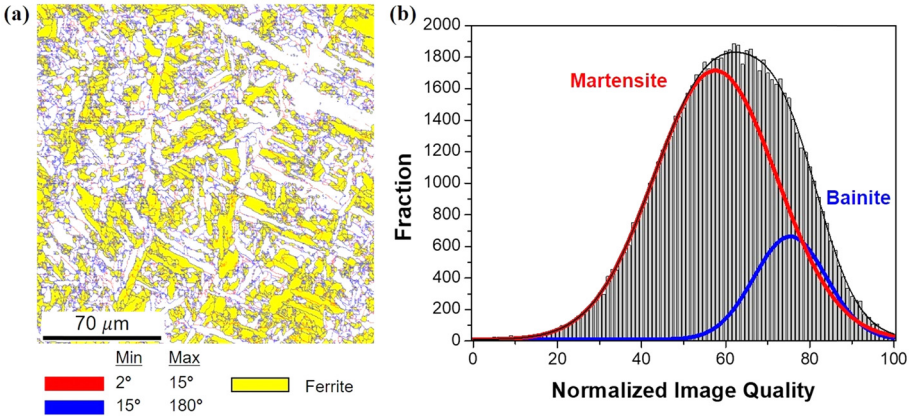

Fig. 6. (a) GOS map (Red and blue lines are low angle grain boundary and high angle grain boundary, respectively) and (b) Normalized IQ Gaussian distribution of sample welded with LTT consumable in weld metal.

blue lines, respectively. Ferrite can be identified in the GOS map, having a tolerance angle of 15 ° and a misorientation angle less than 5 ° [42]; it is represented by the yellow region in Fig 6(a). After eliminating the ferrite phase, bainite and martensite phases can be distinguished by Gaussian fitting the graph from IQ analysis [36]. In general, the martensite phase has larger lattice imperfections than the bainite phase, and thus has lower Kikuchi pattern intensity, which in turn results in lower contrast than the bainite phase [36].

Since the IQ value is affected by many operating factors including image condition, it should be normalized to minimize error effects. The normalized IQ value can be represented by Eq. (3) [43]:

$$IQ_N = \frac{IQ_{Initial} - IQ_{Min}}{IQ_{Max} - IQ_{Min}} \times 100 \quad (3)$$

where IQ_N is the normalized IQ value and $IQ_{initial}$ is the value obtained directly from experiment; IQ_{Max} and IQ_{Min} are the maximum and minimum IQ values.

Figure 6(b), showing the fraction of the normalized IQ value, can be separated into two distributions by Gaussian fitting. The red distribution of IQ values with relatively low contrast represents the martensite phase, and the other distribution of IQ values with high contrast on the right can be identified as the bainite phase.

The phase fractions of ferrite, austenite, martensite and bainite were 50.5%, 0.2%, 40.2% and 9.1%, respectively. The fraction of martensite is considered a major factor affecting the mechanical properties (strength, hardness and toughness) and residual stresses.

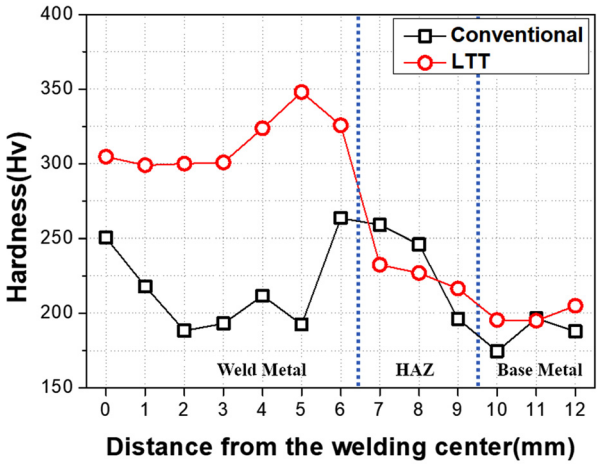

Fig. 7. Results of micro hardness (0.1 kgf) distribution of weldment in the cross-section.

3.2 Micro Vickers hardness and impact toughness

Micro Vickers hardness was evaluated at 1 mm intervals from the weld center to the base metal in the transverse direction for a cross section about 1 mm from the top surfaces of the welding coupons. Similar levels of hardness in the HAZ and base metal were measured as shown in Fig. 7, whereas average hardness values in the weld metal showed a difference, with 216.8 Hv in the conventional consumable and 314.5 Hv in the LTT consumable. Martensite in the LTT weld metal is reasonably considered a major cause of the higher hardness distribution.

The average values of impact absorption energy for the

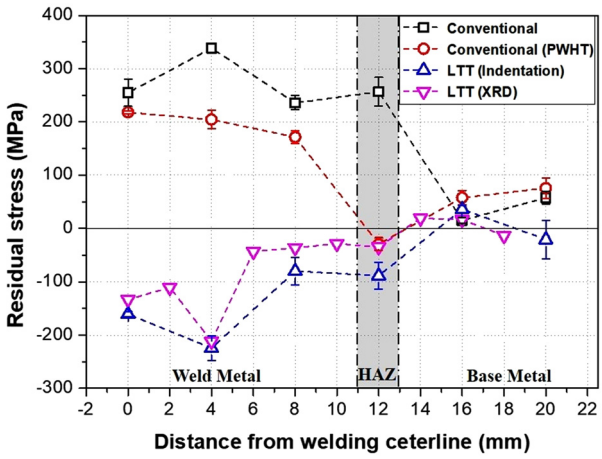

Fig. 8. Averaged residual stresses in the longitudinal and transverse directions on the welding line measured by using indentation and XRD in samples.

conventional weld were 174.3±13 J and 53.3±3 J for the LTT weld. The large difference in impact absorption energy can be explained by microstructure: the greater fraction of acicular ferrite in the material increases impact toughness [44] and finer effective grain size decreases impact toughness [45].

Martensite or martensite-austenite is the main factor determining absorption energy at room temperature, because cracks can initiate due to stress concentrations around a hard phase. The absorption energy can be lower with the higher phase fractions [45,46]. With a conventional consumable, acicular ferrite is distributed and martensite is not present in the weld metal. However, when the LTT consumable was used, a considerable martensite phase was distributed. The presence of these phases influences the difference in impact toughness between the two weldments.

3.3 Residual stress distribution

Figure 8 shows the results of residual stress measurements for three welded coupons. The heat-treated welding coupon with the conventional consumable is included to compare the residual stress distribution of the LTT weld with the distribution after relaxation by PWHT. The stress-relaxing effect was also compared using two coupons welded with a conventional consumable with and without PWHT.

In addition, for the samples welded with the LTT consumable, the residual stress was evaluated using X-ray diffraction and indentation testing to compare the accuracy of the results. The residual stress obtained from indentation is an average value that reflects the stress in the longitudinal and transverse directions on the welding line. In X-ray diffraction, the residual stresses were measured in the longitudinal and transverse directions and the average value was calculated for comparison with the indentation results.

The maximum average residual stress was 339 MPa in the weld metal of the conventional consumable without PWHT. This tensile residual stress is a typical stress distribution that occurs when the thermal shrinkage during the cooling process after welding is a dominant factor. The stress in the weld metal of the heat-treated coupon was about 200 MPa, clearly showing the stress-relieving effect of PWHT. The effect was greater in the HAZ: the stress changed from 257 MPa to -29 MPa. Comparison of the two coupons with and without PWHT emphasize the importance of PWHT on residual stress, especially for the weld metal and HAZ.

The residual stress in the coupon welded with the LTT consumable showed a similar distribution in the results of X-ray diffraction and indentation testing, within a range of 53 MPa. The agreement of the two methods clearly confirms the effect of the LTT consumable. The difference is believed to arise from the difference in measurement depth and area. 50 kgf indentation for a depth less than 100 μm senses the residual stress at depths up to 1 mm, quite different from the X-ray diffraction penetration depth for carbon steel.

For the weldment welded with the LTT consumable, compressive residual stress was distributed in the weld metal and HAZ. Strain in volume expansion due to martensitic transformation at a relatively low temperature was a dominant factor. The martensite phase remaining in the LTT weld metal, as confirmed by microstructural analysis, resulted in the compressive residual stress.

The effect of residual stress on fatigue strength has been investigated by many researchers. The presence of considerable tensile residual stress in welds with conventional consumables with and without PWHT is expected to reduce the fatigue resistance of the joint. On the other hand, it was confirmed that compressive residual stress increases fatigue life [21,27]. Utilizing a Mn-based LTT consumable in the weld can improve fatigue life, like other LTT consumables, and also eliminate the need for PWHT.

4. Conclusions

In this study, the effect of welding consumables (Mn-based LTT and conventional) and PWHT for FCAW-welded ASTM A516-70N carbon steel was analyzed in terms of microstructure, mechanical properties and residual stress. The conclusions are summarized as:

(1) The microstructures containing acicular ferrite, allotriomorphic ferrite, and Widmanstätten ferrite were distributed in the weld metal with the conventional consumable. In the Mn-based LTT consumable weld metal, ferrite, austenite, martensite, and bainite were identified in fractions of 50.5%, 0.2%, 40.2% and 9.1%, respectively, by GOS mapping and normalized EBSD image quality analysis.

(2) The average hardness in the weld metal was 216.8 HV in the conventional consumable and 314.5 HV in the LTT consumable; likewise, the absorption energy from Charpy V-notch testing was 174.3 J and 53.3 J, respectively. For the LTT consumable, the relatively higher hardness and lower absorption energy than the conventional consumable are attributed to the finer effective grain size and the martensite phase.

(3) The residual stress distribution with the LTT consumable was double-checked using two methods, instrumented indentation and X-ray diffraction. The residual stress distributions obtained with both methods showed a similar trend within a range of 53 MPa difference.

(4) Considerable tensile residual stresses were distributed in the coupons with the conventional consumable. PWHT considerably decreased the magnitude of residual stress in the weld metal and the HAZ, especially the HAZ, from 257 MPa to -29 MPa. Compressive residual stress was identified in the weld metal and HAZ when the LTT consumable was used, and this can be presented as the main advantage of the low-transformation-temperature welding consumables.

Acknowledgements

This work was supported by POSCO and the Korea Institute of Energy Technology Evaluation and Planning (KETEP) and the New Faculty Startup Fund from Seoul National University for S.-K. K.

REFERENCES

1. H. Murakawa, M. Béreš, C. M. Davies, S. Rashed, A. Vega, M. Tsunori, K. M. Nikbin, and D. Dye, *Sci. Technol. Weld. Join.* **15**, 393 (2010).
2. D. Deng and H. Murakawa, *Comput. Mater. Sci.* **78**, 55 (2013).
3. G. A. Webster and A. N. Ezeilo, *Int. J. Fatigue* **23**, 375 (2001).
4. S. Zabeen, M. Preuss, and P. J. Withers, *Acta Mater.* **83**, 216 (2015).
5. H. J. Lee, S. Oh, and H. Kim, *Korean J. Met. Mater.* **57**, 51 (2019).
6. H. Murakawa, M. Béreš, A. Vega, S. Rashed, C. M. Davies, D. Dye, and K. Nikbin, *Trans. JWRI* **37** (2008).
7. D. J. Smith and S. J. Garwood, *Int. J. Press. Vessels Pip.* **51**, 241 (1992).
8. J. S. Porowski, W. J. O'Donnell, M. L. Badlani, and E. J. Hampton, *Nucl. Eng. Des.* **124**, 91 (1990).
9. J. Altenkirch, A. Steuwer, M. J. Peel, P. J. Withers, S. W. Williams, and M. Poad, Metall. *Mater. Trans. A* **39**, 3246 (2008).
10. G. Hammersley, L. A. Hackel, and F. Harris, *Opt. Lasers. Eng.* **34**, 327 (2000).
11. Hyeonuk Park, Junhyung Kim, Youngsik Pyun, Amanov Auezhan, Yoon Suk Choi, *Met. Mater. Int.* **25**, 606 (2019).
12. WKC. Jones and PJ. Alberry, *Met. Technol.* **11**, 557 (1977).
13. J. Altenkirch, J. Gibmeier, A. Kromm, T. Kannengiesser, T. Nitschke-Pagel, and M. Hofmann, *Mater. Sci. Eng. A* **528**, 5566 (2011).
14. A. Ohta, N. Suzuki, Y. Maeda, K. Hiraoka, and T. Nakamura, *Int. J. Fatigue* **21**, S113 (1999).
15. W. Wang, L. Huo, Y. Zhang, D. Wang, and H. Jing, J. *Mater. Sci. Technol.* **18**, 527 (2002).
16. P. P. Darcis, H. Katsumoto, M. C. Payares-Asprino, S. Liu, and T. A. Siewert, *Fatigue Fract. Eng. Mater. Struct.* **31**, 125 (2008).
17. S. Zenitani, N. Hayakawa, J. Yamamoto, K. Hiraoka, Y. Morikage, T. Kubo, K. Yasuda, and K. Amano, *Sci. Technol. Weld. Join.* **12**, 516 (2007).
18. A. Kromm and T. Kannengiesser, *Soldag. insp.* **14**, 82 (2009).
19. A. Ota, C. Shiga, Y. Maeda, N. Suzuki, O. Watanabe, T. Kubo, K. Matsuoka, and S. Nishijima, *Weld. Int.* **14**, 801 (2000).

20. J. Eckerlid, T. Nilsson, and L. Karlsson, Sci. Technol. *Weld. Join.* **8**, 353 (2003).
21. A. Ohta, N. Suzuki, Y. Maeda, and S. J. Maddox, *Weld. World* **47**, 38 (2003).
22. E. Harati, L. Karlsson, L.-E. Svensson, and K. Dalaei, *Int. J. Fatigue* **97**, 39 (2017).
23. H. K. D. H. Bhadeshia, Math. Modell. *Weld Phenom.* **2**, 71 (1995).
24. Y. Mikami, Y. Morikage, M. Mochizuki, and M. Toyoda, *Sci. Technol. Weld. Join.* **14**, 97 (2009).
25. A. Kromm, J. Dixneit, and T. Kannengiesser, *Weld. World* **58**, 729 (2014).
26. X. Chen, P. Wang, Q. Pan, and S. Lin, *Cryst.* **8**, 293 (2018).
27. Z. Barsoum and M. Gustafsson, *Eng. Fail. Anal.* **16**, 2186 (2009).
28. H. K. D. H. Bhadeshia, *Mater. Sci. Eng. A* **378**, 34 (2004).
29. IIW/IIS DOC. 452-74. *Weld World* **12**, 65 (1974).
30. AWS—A5.20/A5.20M:R2015 Carbon Steel Electronics for Flux Cored Arc Welding; (AWS: Miami, FL, USA, 2015).
31. ASME Section III, NX, "Rules for Construction of Nuclear Facility Components", ASME, 2010.
32. ASME Boiler and Pressure Vessel Code, Section II SA-370, 2015.
33. ISO/FDIS 14577-1: Metallic materials - Instrumented indentation test for hardness and material parameter, Part 1: Test method. (International Organization for Standardization, Geneve, Switzerland, 2002).
34. ASTM E2546-15: Standard Practice for Instrumented Indentation Testing (ASTM International, 2015).
35. Y.-H. Lee and D. Kwon, *Acta Mater.* **52**, 1555 (2004).
36. M.-S. Baek, K.-S. Kim, T.-W. Park, J. Ham, and K.-A. Lee, *Mat. Sci. Eng. A* **785**, 139375 (2020).
37. M. Abbas, A. S. Hamdy, and E. Ahmed, *Mater. Res. Express* **7**, 036523 (2020).
38. T. W. Shin, J. H. Hyun, and J. H. Koh, *J. Weld. Join.* **35**, 68 (2017).
39. N. J. Kim and Y. G. Kim, *Mater. Sci. Eng. A* **129**, 35 (1990).
40. Y. Ohmori, H. Ohtani, and T. Kunitake, *Met. Sci.* **8**, 357 (1974).
41. N. Isasti, D. Jorge-Badiola, M. Taheri, B. López, and P. Uranga, *Metall Mat Tras.* **42**, 3729 (2011).
42. S.-I. Lee, T.-W. Hong, and B. Hwang, *Korean J. Mater. Res.* **27**, 636 (2017).
43. J. Wu, P. J. Wray, C. I. Garcia, M. Hua, and A. J. Deardo, *ISIJ Int.* **45**, 254 (2005).
44. L. Svensson and B. Gretoft, *Weld. J.* **69**, 454 (1990).
45. S.-W. Lee, S.-I. Lee, and B. Hwang, *Korean J. Met. Mater.* **58**, 293 (2020).
46. N. Huda, A. R. H. Midawi, J. Gianetto, R. Lazor, and A. P. Gerlich, *Mater. Sci. Eng. A* **662**, 481 (2016).